A new approach to thermal history modelling with detrital low temperature thermochronological data

Kerry Gallagher, Mauricio Parra

Elsevier Editorial System(tm) for Earth and Planetary Science Letters

Manuscript Draft

Manuscript Number: EPSL-D-19-01000R1

Title: A new approach to thermal history modelling with detrital low temperature thermochronological data

Article Type: Letters

Keywords: detrital thermochronology; thermal history; inversion

Corresponding Author: Professor Kerry Gallagher,

Corresponding Author's Institution: University of Rennes 1

First Author: Kerry Gallagher

Order of Authors: Kerry Gallagher; Mauricio Parra

Abstract: We present an inverse modelling strategy to infer thermal history information from detrital low temperature thermochronological data from modern sediment sampling the outlet of a single catchment. As presented, the method relies on the assumption that the geological timescale thermal history was the same across the catchment. The detrital sample is assumed to represent a mixture of grains originating from a potentially unknown sampling of the present elevation range in the catchment. The approach also implements a method to infer a function describing the topographic sampling represented in the detrital sample. In practice, this may reflect variations in erosion with elevation but also lithological differences in the catchment (fertility) and the nature of erosion/transport processes in the catchment. A combination of detrital and in-situ bedrock data are recommended to improve the resolution of the topographic sampling function. We demonstrate the application of the approach to aset of fission track data from the Fundacion catchment in the Sierra Nevada de Santa Marta in northern Colombia. The inferred thermal history suggest a period of rapid cooling initiated around 50-30 Ma, followed by slower cooling to the present day, consistent with the regional geological history. The topographic sampling function estimates suggest that the hypsometric distribution is not appropriate in terms of the contributions from different elevations to the detrital sample. Rather, the data imply a higher proportion of sampling from lower elevations close to the location of the outlet where the detrital sample was collected.

A new approach to thermal history modelling with detrital low temperature thermochronological data

Kerry Gallagher[1] and Mauricio Parra[2]

1. Géosciences Rennes/OSUR, University of Rennes, Rennes, 35042, Rennes, France

kerry.gallagher@univ-rennes1.fr

2. Institute of Energy and Environment, University of São Paulo, Av. Prof. Luciano Gualberto 1289, Cidade Universitária, 05508-010, Sao Paulo-SP-Brazil

mparra@iee.usp.br

Corresponding author : Kerry Gallagher (kerry.gallagher@univ-rennes1.fr).

Abstract

We present an inverse modelling strategy to infer thermal history information from detrital low temperature thermochronological data from modern sediment sampling the outlet of a single catchment. As presented, the method relies on the assumption that the geological timescale thermal history was the same across the catchment. The detrital sample is assumed to represent a mixture of grains originating from a potentially unknown sampling of the present elevation range in the catchment. The approach also implements a method to infer a function describing the topographic sampling represented in the detrital sample. In practice, this may reflect variations in erosion with elevation but also lithological differences in the catchment (fertility) and the nature of erosion/transport processes in the catchment. A combination of detrital and in-situ bedrock data are recommended to improve the resolution of the topographic sampling function. We demonstrate the application of the approach to a set of fission track data from the Fundación catchment in the Sierra Nevada de Santa Marta in northern Colombia. The inferred thermal history suggest a period of rapid cooling initiated around 50-30 Ma, followed by slower cooling to the present day, consistent with the regional geological history. The topographic sampling function estimates suggest that the hypsometric distribution is not appropriate in terms of the contributions from different elevations to the detrital sample. Rather, the data imply a higher proportion of sampling from lower elevations close to the location of the outlet where the detrital sample was collected.

Keywords : Detrital thermochronology, thermal history, inversion

1. Introduction

Since the seminal papers defining the concept and calculation of closure temperature (Dodson, 1973) and early applications of the concept (e.g. Wagner et al. 1977), one of the main uses of temperature dependent geochronology, or thermochronology is to recover information on the thermal histories of rocks. In doing this we exploit the fact that different dating systems, defined by a combination of a specific mineral and isotope decay scheme, are sensitive to different temperature ranges. This temperature sensitivity is generally manifested in terms of losing the daughter product by some kind of thermally activated diffusion process, and leads to a measured age younger than the formation age of the host rock. For high temperature systems such zircon U-Pb, the measured age is often interpreted as the time at which the host rock cooled below the appropriate closure temperature. The closure temperature is a function of cooling rate, grain size and dating system specific kinetic and geometry parameters as defined by Dodson (1973) and for zircon U-Pb is nominally around 1000-1100°C (e.g. Schoene 2014).

Low temperature thermochronology is typically defined to include apatite and zircon (U-Th)/He and $^{4}He/^{3}He$ dating, apatite and zircon fission track analysis and feldspar K-Ar and $^{40}Ar/^{39}Ar$ dating (see Reiners and Ehlers, 2005). These particular systems are sensitive to temperatures from near surface temperatures (~30-40°C) to a maximum around 400°C but are also characterised by a large range in temperature sensitivity relative to the nominal closure temperature, referred to as the partial annealing zone for fission track analysis and the partial retention zone for noble gas diffusion. This range in temperature sensitivity, and so loss of daughter product, is then manifested as a progressive decrease in measured age depending on how long a given rock sample has resided in, or has taken to cool across, the partial retention/annealing zone.

For surface or bedrock samples collected from different elevations in a given catchment or valley, this effect is typically represented as a vertical profile in which age increases with elevation (e.g. Wagner and Reimers, 1972, Fitzgerald, et al. 1995, Valla et al. 2010). Often there is a change inferred in the slope of the age-elevation relationship, such that the lower part of the profile has a steeper slope than the upper part. This can be interpreted as either a change in erosion rate, an exhumed partial retention/annealing zone or more generally as a combination of both. Such interpretations can be made in a relatively qualitative sense (e.g. Fitzgerald et al. 1995), or in a more quantitative sense, typically involving the inference of the cooling and/or erosion history through forward or inverse thermal history modelling (Ehlers 2005, Gallagher et al. 2005, Valla et al. 2010, Braun et al. 2012, Fox et al. 2014).

As it is generally erosion that controls the cooling history recorded in low temperature thermochronometers, an obvious extension of the vertical profile approach is to consider the products of erosion, i.e. detrital thermochronology. Early applications of detrital thermochronology considered distributions of single grain ages from sediments for different closure temperature systems such as zircon U-Pb, mica and feldspar $^{40}Ar/^{39}Ar$, or zircon and apatite helium dating or fission track analysis, and relating these to possible source regions over geological time (e.g., Ross and Bowring 1990, Copeland and Harrison 1990, Garver and Brandon 1994, Carter and Bristow 2000, Tranel et al. 2011, Enklemann and Ehlers 2015, Malusà and Fitzgerald 2019).

Furthermore, efforts have been made to exploit the distribution of detrital ages measured in modern sediments to inform us about the nature of erosion and tectonic processes in the recent geological past by predicting the expected distribution of detrital ages for a range of thermochronometric systems, including some of the lower temperature systems such as apatite (U-Th-Sm)/He (AHe) and apatite fission track (AFT) data. These predictions are often made using local vertical age profiles (Brewer et al., 2003, Ruhl and Hodges 2005, Stock et

al. 2006, Huntington and Hodges 2006, Malusà and Fitzgerald 2019) or using predictions as a 2D age-elevation surface, the ages being predicted from landscape and/or 3D thermal models (e.g. Whipp et al 2009, Ehlers et al. 2015). These approaches require some form of assumptions, either *a priori* or *a posteriori*, about the nature of sampling of the age-elevation distribution. This has commonly been taken to be the hypsometric distribution by default. In this case, the detrital ages are assumed to be a mixture of ages from either a predicted or observed age-elevation relationship, sampled according to the proportion of the present topography in a given elevation range over the area of the relevant catchment or drainage basin. A different approach was implemented by Avdeev et al. (2011) and Fox et al. (2015) in which they inferred a distribution of age-elevation relationships and how these could be sampled over different elevations, as a function of variable erosion rate, to reproduce both detrital and in situ bedrock age data. More recently, Braun et al. (2018) and Gemignani et al (2018) proposed a form of statistical un-mixing of downstream variations in measured detrital ages which does not require any assumption about the sampling of topography. However, this approach requires multiple detrital samples and the drainage system to traverse several (sub)-catchments, or regions, contributing different cooling signals to the final distribution.

Here we propose an inverse method to infer the thermal history from a modern detrital sample from a single catchment. In this case, the implicit assumption is that any thermal history information recorded in the modern sediment reflects the same long term thermal history experienced by bedrock samples in the catchment. The motivation for this approach is firstly to assess whether modern detrital samples can provide similar thermal history information as a typical bedrock vertical profile. A lack of bedrock samples occur due to the inaccessibility of some source regions, e.g. under ice as highlighted by Enkelmann and Ehlers (2015), or for logistical reasons (cost, access). In the absence of bedrock samples, we will need to make an assumption about how erosion processes sample the present day catchment

topography. We will use the phrase topographic sampling function (TSF) to describe the sampling of the in situ or bedrock vertical profile data to produce modern sediment detrital data. To relax the assumption that we know *a priori* this topographic sampling function, the method we present allows us to treat this as an unknown. As we will focus on low temperature thermochronometers, specifically apatite fission track analysis and apatite (U-Th-Sm)/He dating, it is important also to note a potential sampling bias related to variable concentrations of a specific mineral (e.g. apatite), or fertility in the source region (e.g. Tranel et al. 2011) and the effects of hydraulic sorting of different grain-size fractions (e.g. Malusà and Garzanti 2019). Thus any inferred topographic sampling function will reflect a combination of modern erosion and transport processes acting on the catchment and the fertility of bedrock outcropping across it.

In the following, we describe the method we have developed to deal with extracting thermal history information from detrital low temperature thermochronological data. Here we focus on AFT and AHe data in particular, but the approach is readily extended to other data types (e.g. ZHe) from the outlet of a given catchment. The detrital data may also be combined with in situ bedrock data (the canonical vertical profile). An implicit assumption is that the distribution of ages with elevation is effectively constant (or has minor and smooth variations). The approach we present also allows us to infer the topographic sampling function. We show that in the case where we have both detrital and vertical profile data, this approach allows us to infer the topographic sampling function with more confidence, than just detrital data alone. Finally, we demonstrate the application of the method to an AFT dataset from northern Colombia.

2. Methodology

The inverse thermal history modelling problem for a 1D vertical profile with in situ bedrock samples has been previously described (Gallagher et al. 2005, Gallagher 2012) so we only briefly review the main assumptions here. All samples in a vertical profile are assumed to have experienced the same general form of thermal history with the difference between the thermal histories for the top and bottom samples defined by a temperature gradient that may vary over time. It is implicit that lower elevation samples can never have been at lower temperatures than higher elevation samples. Therefore, a vertical profile can not be cut by faults active over the timescale relevant to the thermal history, nor can the thermal state of the bedrock have been locally perturbed, for example by hot fluid circulation. For a given thermal history we can make a prediction of the AHe/AFT age and track length distribution elevation profiles by exploiting the appropriate diffusion/annealing models. By suitably combining the predictions over the elevation range of a given catchment, we can similarly make a prediction of the detrital age distribution. Thus, the detrital data can be considered as a sampling of the vertical profile data in the catchment. It is important to highlight that dispersion in such detrital data will reflect the combination of grains from different elevations (hence different thermal histories), but factors controlling the rates of annealing (AFT) and diffusion (AHe) for each grain and also different sources of measurement error. Therefore, dispersion in AFT data can occur due to variations in annealing kinetics attributable to chemical composition, e.g. Cl content or a proxy compositional measure such as Dpar (Green 1988, Ketcham et al., 1999, 2007), as well as the statistical variability of single grain-ages inherent in the track counting process (e.g. Galbraith 2005). We allow for these factors in the method we present here. AHe data can show dispersion due to variation in whole grain geometries and sizes (e.g. Farley, 2000), the presence of broken grains (Brown et al. 2013,), and variable diffusion kinetics due to radiation damage related effects (Flowers et al. 2009; Gautheron et al. 2009,

Willet et al. 2017). Here, we allow for variable grain size, but not the effects of radiation damage on He diffusion in apatite nor incomplete or broken apatite grains. However, the general methodology we present could deal with both of these factors at the expense of increased computation time.

2.1 The forward problem

The general forward problem is illustrated in figure 1 (and see also Gallagher 2012). We initially specify the model (***m***) as a thermal history, given by a series of time-temperature points and the temperature difference, or temperature gradient, between the uppermost and lowermost elevations in a hypothetical vertical profile that covers the maximum range of elevation in the catchment . Combined with the appropriate diffusion/annealing models, we can make a prediction of the age/length-elevation profiles. As a consequence of the factors leading to dispersion described above, these will be distributions, rather than point values, at a given elevation. These distributions need to be propagated into the predicted final detrital age/length distributions. To generalise, we will refer to the kinetic parameter and grain size variables as control variables and these will be represented by κ and the range of possible values defined by κ_{min} and κ_{max}. In the following, we will present the approach considering just one general control variable. Then we can write the total predicted detrital distribution, conditional on the thermal history model, ***m*** , as

$$p_{detrital}(d_p) = \int_{\kappa_{min}}^{\kappa_{max}} \int_{z_{min}}^{z_{max}} d_p\,(z, \kappa \lfloor m) p(z) p(\kappa)\, dz\, d\kappa \qquad (1)$$

where $d_p(z, \kappa \lfloor m)$ is the predicted distribution for elevation z and control parameter value κ, $p(\kappa)$ is the probability distribution on the control variable, and *p(z)* is the probability of sampling from elevation z, or what we refer to above as the topographic sampling function

(TSF). Often the TSF is assumed to be equivalent to the hypsometric distribution. We return to this later, but for the moment we state that if we specify a thermal history and the TSF in a catchment, we can predict what age/length distributions we expect to see in a detrital sample with grains from that catchment.

2.1.1 Predicting the AFT age and length distributions

For a given thermal history and kinetic parameter, we predict the noise-free fission track age and length distribution at a given elevation. For the age, we use the external detector method (EDM) age equation (e.g., Hurford and Green, 1983) to calculate the spontaneous to induced track density ratio, ρ_s/ρ_i for a given thermal history. We can convert the predicted AFT age into the equivalent ρ_s/ρ_i. Following Galbraith (2005) and Gallagher (1995), we use a binomial distribution to sample values of the spontaneous to induced track counts ratio N_s/N_i. The parameter of the binomial distribution is given as

$$\theta = \frac{\rho_s/\rho_i}{1 + \rho_s/\rho_i} \tag{2a}$$

and given a selected total number of track counts, $N_s + N_i$, the probability for the number of spontaneous tracks is given as

$$p(N_s|N_s + N_i) = \frac{(N_s+N_i)!}{N_s!N_i!}\,\theta^{N_s}(1-\theta)^{N_i} \tag{2b}$$

We choose a given number of ages to sample (e.g. up to 100 grain ages for a given compositional group at each elevation), randomly select $N_s + N_i$ (from a specified range, e.g. 50 and 500, or based on the range of values measured in a detrital sample), then randomly sample for N_s from the binomial distribution. The result gives a value of N_s/N_i which can then be converted into an AFT age and the error using the standard EDM error equation. We

repeat this process for the specified number of sampled ages and the predicted distribution is then calculated by summing all the individual Gaussian distributions defined with the mean equal to the individual AFT age and the calculated error as the standard deviation. Alternatives to assuming a Gaussian kernel for each individual age include assuming N_s/N_i is distributed as a Gaussian, or that, for a given $N_i + N_s$, $N_s$is binomially distributed (Brandon 1996, Galbraith 2005). The process of adding kernel distributions gives a continuous predicted AFT age distribution for a given apatite kinetic parameter at a given elevation accounting for the Poissonian variation of single-grain ages expected due to the counting process. The AFT track length distributions are similarly predicted directly from the forward model (e.g. Green et al. 1989, Gallagher 1995, Ketcham et al 1999) for each kinetic parameter group and elevation. Next, both the age and length distributions at each elevation are then combined for all control variable groups using a weighting based on the number of grains/lengths in each kinetic parameter group. In practice, these groups are defined from the measured values in the actual detrital sample. Finally, we combine the elevation dependent distributions using the TSF as weights to produce the final detrital distribution for the AFT data.

2.1.2 Predicting the AHe age distribution

For a given thermal history, we predict the noise-free AHe age as a function of elevation and grain size, using the spherical grain equivalent radius (Farley 2000). To predict a distribution of ages for a given elevation and grain size, we resample a Gaussian distribution with a mean defined by the predicted AHe age and a standard deviation of 10% of the calculated age error to produce 50 single grain ages for each grain size group at each elevation. These are then combined using a weighting, again based on the number of grains in each grain size group in the actual detrital sample. Finally, we combine the elevation dependent distributions using the TSF as weights to produce the final detrital distribution for the AHe data.

2.2 Inverse problem

The inverse problem is stated as follows: if we have a set of measured detrital AFT and AHe data from a single catchment, we want to recover the catchment thermal history and also potentially the topographic sampling function. We define the observed detrital data as $\mathbf{d} = (d_1,d_2...d_i,...d_N)$, a vector of length N, made up of a N_c AFT single grain ages, N_l track length data and N_{He} AHe single grain ages, each with some form of explicit or implicit measure of uncertainty (e.g. a reported measurement error on an AHe age, an assumed measurement error on a track length, or a Poisson related distribution associated with track counts). We use the forward model approach described above to predict the age/length distributions as a function of elevation over the maximum elevation range of the catchment. The approach we present can also incorporate any available bedrock vertical profile data in the catchment generally allowing better inference of both the thermal history and the topographic sampling function.

2.2.1 Inference of the thermal history

For the moment, we concentrate just of the thermal history inference problem. We implement the same form of transdimensional Bayesian Markov chain Monte Carlo (McMC) algorithm described in Gallagher (2012) and we will not repeat the details. In brief, the thermal history parameters are defined as an unknown number of time temperature points, each point with an associated temperature gradient which may be specified to be constant or variable over time. The prior distributions for these thermal history parameters are defined to be uniform, i.e. equal probability between an upper and lower limit.

Given a thermal history model, and using d_p as a prediction (age or length) for that model, we define total predicted detrital age or length distribution for a given elevation and control variable, κ_j, as $p(d_p|\kappa_j, z)$. This can be integrated over elevation with the TSF (= *p(z)*) as

$$p_{detrital}(d_p|\kappa_j) = \int_{z_{min}}^{z_{max}} p\,(d_p|\kappa_j, z)p(z)dz \quad (3)$$

To reduce the computational time, we can calculate the distributions for a finite number of control variable groups at a finite number of elevations. Then we can write the equation above in discrete form as

$$p_{detrital}(d_p|\kappa_j) = \sum_{k=1}^{N_z} p\,(d_p|\kappa_j, z_k)p(z_k) \quad (4)$$

where N_z is the number of elevation groups, which is selected to cover the range of topography in the catchment of interest and we assume $p(z_k)$ is constant for each elevation group, defined by the range $z_{(k-1)/2} > z_k > z_{(k+1)/2}$ and $z_{(k-1)/2}$ is the midpoint between z_{k-1} and z_k and a similar definition for $z_{(k+1)/2}$.

Following on from this, we can write the total predicted detrital age or length distribution, summed over the control variables (with probability distribution $p(\kappa_j)$) as

$$p_{detrital}(d_p) = \sum_{j=1}^{N_\kappa} p\,(d_p|\kappa_j)p(\kappa_j) \quad (5)$$

where N_κ is the number of control variable (e.g. compositional or grain size) groups, which can be based on the range of values in a given detrital sample, and $p(\kappa_j)$ is a distribution based on the number of samples with a value in a range defined by $\kappa_{j,min} < \kappa_j < \kappa_{j,max}$. We can either assign an observed datum to a given control variable group (which we do for AFT age and length data using a kinetic parameter, e.g., Cl, Dpar), or using the upper and lower limits for the group bounding a given control variable value, we can interpolate the

predictions for the specific value for a given grain (which we do for AHe age data for grain size).

2.2.2 Estimating the Topographic Sampling Function (TSF)

We can exchange the order of the summation in equation (4) and write

$$p_{detrital}(d_p|z_i) = \sum_{j=1}^{N_k} p\,(d_p|\kappa_j, z_k)p(\kappa_j) \quad (6)$$

and

$$p_{detrital}(d_p) = \sum_{k=1}^{N_z} p\,(d_p|z_k)p(z_k) \quad (7)$$

From this we see there is a linear relationship between the predicted detrital distribution, integrated over the range of control variables, and the topographic sampling function (*p(z)* above). This lets use a linear inverse method to estimate the latter. The only complication is that $p(z) \geq 0$, so we implement the iterative non-negative least squares method presented by Kim et al. (2013). This gives an optimal TSF in the least squares sense in that it minimises the sum of squares between the predicted and observed detrital distributions. Another approach to infer the TSF is to implement a probabilistic McMC sampling method as used by Avdeev et al. (2011) and Fox et al. (2015) to constrain erosion rate over elevation with detrital thermochronology, or more generally in change point modelling by Gallagher et al (2011). This approach can directly represent the TSF as a weighting function over a given elevation range, and using transdimensional sampling, it is possible to assess the required complexity of the TSF. At this stage, we have not fully implemented this approach, as it proves to be considerably more computationally intensive that the optimal least squares approach mentioned above.

The elevations where we calculate the age or length distributions do need not correspond to the elevations used to define the topographic sampling function (e.g. this could be the hypsometric distribution defined at regular elevation intervals). As the predicted distributions for a given control variable and elevation are smooth, we can interpolate the predicted discrete ages or distributions to the intermediate elevations. We do this interpolation using the approach described in Read (1999), which relies on weighted linear interpolation between the cumulative distributions.

2.2.3 The likelihood function

In general terms, the likelihood is a measure of how well predictions from a given model represent the observed data. This can be defined (up to a constant of proportionality) as the probability of having the observed data, given the predictions from a given (thermal history and topographic sampling function) model. For the detrital data, we use the predicted detrital age and length distributions to form the likelihood function. In the following, the distributions are all normalised so they integrate to one, and can be treated as probability distributions.

If we consider detrital AFT data first, the i-th observation, d_i, from the j-th control variable group j , κ_j, will be either a fission track single grain age or an individual track length measurement and the control variable group will be defined as a range of some kinetic parameter such Cl content or Dpar. In practice, we use the mean of the kinetic parameter in the appropriate range to make the predictions for that kinetic parameter group as described earlier, and this distribution is used for all observed data relevant to that group. For AHe age data, we use the same interpolation procedure mentioned above such that, for a given measured radius, we interpolate between the 2 distributions predicted for the two radii that bracket the measured radius. The interpolated distribution, appropriate for the actual effective grain radius, is used as the likelihood function for that grain. To incorporate additional control

variables, such as radiation damage controlled diffusion, typically parameterised by models based on effective uranium (eU) (e.g. Flowers et al; 2009, Gautheron et al. 2009), we would follow a similar approach defining a range of eU values based on those in the detrital sample. The likelihood for a given AHe age could then be based on 2D interpolation of the predicted ages as a function of grain size and eU.

The likelihood for a single datum, d_i, given the thermal history model, $p(d_i|m)$, can be defined as the integral or sum of the predicted distributions over elevation, for the appropriate control variable value, weighted by the topographic sampling function, $p(z_k)$, for elevation , z_k

$$p(d_i|m) = \sum_{k=1}^{N_z} p\,(d_i|\kappa_j, z_k, m)p(z_k) \quad (8)$$

Here we have dropped the dependence on κ_j on the left hand side as it is implicit for the given observation.

The definitions of the likelihood functions implicitly allow for the possibility that the probability of an observed value, with its associated control variable, may be zero over a range of elevations, i.e. the predicted distributions over that elevation range do not include the value of that observation.

The total likelihood is the product of all the individual likelihoods for each individual observation, given as

$$p(d|m) = \prod_{i=1}^{N} p(d_i|m) \quad (10a)$$

In practice, the preference is to use the log likelihood, defined as

$$L(d|m) = \sum_{i=1}^{N} Ln(p(d_i|m)) \quad (10b)$$

The methodology described here has been implemented in the software QTQt, and so the inversion approach for the thermal history, implementing trans-dimensional Markov chain Monte Carlo, closely follows given in Gallagher (2012). This implementation readily allows detrital data and the classical in situ (bedrock) vertical profile data to be combined, as we just need to add the individual sample log likelihood values for a given thermal history.

3. Application to real data

To demonstrate the application of the methodology described above, we give results using synthetic AHe and AFT data in the supplementary material, showing the approach works. Here we focus on a data set from the Fundación catchment in the Sierra Nevada de Santa Marta in northwest Colombia (see figure 2a). This catchment an ideal location for testing our method, given its small size (~14,500 km^2), high relief (~4 km), a relatively homogeneous lithology with abundance of apatite-rich granitoids and gneisses and a combination of in situ and detrital AFT data. The present day elevation in the catchment ranges from 180 to 3900 m and in figure 2b, we show the present day hypsometry, as a cumulative distribution, which shows that less than 20% of the topography is above 2500 m. Villagomez et al. (2011) reported AFT data from 9 samples forming a vertical profile over an elevation range from 300 to 2700 m (Table S1, supplementary material). For logistical reasons, it was not possible to collect samples from the last 1200 m. We have also recently produced a new suite of detrital 99 AFT single grain ages and 21 track length (and angle to c-axis) measurements from a

363 sample collected at the outlet of the catchment (Parra et al., in press, Tables S2, S3,
364 supplementary material). This combined data set lets us compare the thermal histories
365 inferred from the vertical profile data alone, the detrital data alone and the two data sets
366 together, as well as the case when we treat the topographic sampling function (TSF) as
367 unknown. We implement the approach described above by using hypothetical or dummy
368 samples located at 300 m intervals over the total elevation range of the Fundación catchment.
369 For a given thermal history, we predict the age and length distributions for these dummy
370 samples at each elevation, and then combine the distributions, weighted by the topographic
371 sampling function, to produce the final predicted detrital age and length distributions.
372 Initially, we fix the TSF to be equivalent to the present day hypsometry and consider only
373 inference of the thermal history. Subsequently, we relax this assumption and allow inference
374 of both the thermal history and TSF.

375 *In situ bedrock data alone*

376 In figure 3a, we show firstly the inferred expected thermal history based on the in situ vertical
377 profile AFT data of Villagomez et al. (2011). The McMC sampler was run for 100,000
378 iterations, and the results presented here are derived from the last (post-burn-in) 50,000
379 iterations. We used the multi-compositional annealing model of Ketcham et al. (2007) with
380 Dpar as the kinetic parameter, with values sampled from a normal distribution with the
381 measured values for the mean and standard deviation as the parameters of the distribution.
382 The inferred thermal history implies a period of rapid cooling between 50 and 30 Ma,
383 followed by a decrease in cooling rate for the uppermost samples. Using the dummy samples
384 at 300 m intervals, with a range of kinetic parameter equivalent to that measured in the
385 detrital sample, we also can predict the range of ages we expect for the dummy samples for all
386 thermal histories accepted by the McMC sampling and these are also shown on figure 3b. The
387 thermal histories, inferred from the in situ data alone, predict a range of AFT ages whose

388 width increases with elevation above the last in situ sample at 2700 m profile. In figure 3c, we
389 show the predicted detrital age distribution for the thermal history in 3a (assuming that the
390 catchment is sampled according to the hypsometric curve). In terms of visual comparison, the
391 predicted distribution is best compared to the continuous distribution (in light blue in figure
392 3c) rather than the histogram. The continuous distribution is a kernel density representation of
393 the observed grain ages and errors, tending to smooth out isolated peaks present in the
394 histogram, which we do not expect the predicted distribution (also a kernel density
395 representation) to reproduce. The predicted distribution in this case has a peak about 20 Ma
396 older than the observed peak, and also lacks the tail of older ages (> 60-70 Ma). These
397 discrepancies could be due to the thermal histories not predicting old enough ages at higher
398 elevation, and/or the topographic sampling function not sampling the predicted vertical profile
399 distributions to capture the older ages at higher elevations.

400 *Detrital data alone*

401 Next we use only the catchment outlet detrital AFT data to infer the thermal history. The main
402 model run parameters were the same as the previous run and we used the hypsometric curve
403 as the TSF to produce the predicted detrital distribution. The results are shown in figure 4.
404 The thermal history also shows a cooling episode starting around 50 Ma, but does not imply a
405 change in cooling rate. As we would expect, the detrital age distribution is better reproduced
406 as just the detrital data were used for the inference of the thermal history. Using this thermal
407 history to predict the in situ vertical profile, the data from lower elevations are less well
408 predicted than the previous example while the data from the upper samples are better
409 reproduced. We can see from figure 4b that the predicted ages above 3000m are generally
410 older, and the range narrower than in the previous case. Consequently, we can reproduce the
411 older ages in the detrital sample, albeit with a relatively small proportion of the total predicted
412 elevation profile being sampled by the hypsometric curve as the TSF.

In situ and detrital data jointly

In this case, we combine the data from the previous two examples in a joint inversion, and again using the hypsometric curve as the TSF. The results are given in figure 5. Relative to the two previous examples, the inferred thermal history is most similar to the detrital data only case, but with the cooling event starting a little earlier, but still around 50 Ma, and a lower implied temperature gradient at that time. Relative to the detrital data only case (fig. 4), the combined data reproduces the detrital age distribution less well (over-predicting the peak age by about 10 Ma) and the vertical profile data better, except perhaps the uppermost in situ sample. The opposite tendencies are the case relative to the in situ only results (fig. 3). Given the previous results, this is not unexpected as some kind of compromise solution between the two solutions based on just the in situ vertical profile or detrital data sets.

In situ and detrital data jointly, and inference of TSF

The results of the previous examples are based on assuming the TSF is given by the hypsometric curve. Now we relax that condition and use the combined in situ and detrital data to infer the TSF. To achieve this we first consider a proposed thermal history, and predict the detrital distributions using the hypsometric curve as an initial TSF model. Then we use the iterative non-negative least squares algorithm of Kim et al. (2013) to estimate a TSF that provide the optimal fit (in the least squares sense) to the observed data. Given this least squares estimate for the TSF, we calculate the likelihood for the detrital data as defined earlier. The combined thermal history-TSF proposed model may or may not be accepted during the McMC sampling, as at any given iteration the acceptance or rejection of a proposed model is effectively based on the likelihood function value relative to that of the current model (the accepted model from the previous iteration). We present an uncertainty range for the least squares TSF estimates that represents the 95% credible interval for all

accepted models. This implied uncertainty can be considered optimistic (too small) as we use only the optimal (non-negative least squares) solutions for each accepted thermal history, rather than a population of estimates that would be obtained with an McMC sampling method, as mentioned earlier.

The results are shown in figure 6. Now, the expected thermal history is most similar to that obtained using just the in situ vertical profile data, but the peak of younger ages in the observed detrital data is better reproduced. Relative to the input hypsometric curve, the inferred topographic sampling function implies a greater contribution from lower elevations, such that 50% comes from < 700m and correspondingly less at the highest elevation. The few older detrital ages are not well predicted for the expected model, but we see the average of all predicted detrital distributions does have a small contribution around 80-90 Ma.

The surface geology shows two main lithological groups, Precambrian gneisses with amphibolite and granulite facies that occupy 22% of the total area and crop out at lower elevations, and Jurassic and Triassic granitoids that constitute the rest of the catchment, at both lower and higher elevations (Figure 2). Both groups contain apatite, as shown by the bedrock data set used in this paper, which include samples from both lithological groups. If we rule out uneven fertility the inferred TSF then implies that it is the contribution from lower elevations that lets us reproduce the young peak in the detrital data. While this makes sense in terms of proximity to the outlet where the detrital sample was collected, and perhaps reflects local river incision, a test of this inference would be to obtain U-Pb ages on the apatite grains, which would clearly distinguish the relative contributions of a Precambrian source from a Triassic-Jurassic source. Furthermore, the fertility in terms of apatite yield vary significantly in the same lithology (e.g. by x100, Tranel et al 2011), and a more detailed assessment of this factor in the source region and its modification during transport would be required to

substantiate this interpretation of the inferred TSF. Finally, we assume that the TSF is the same for the same elevations across the catchment.

The geological interpretations of the thermal history models are beyond the scope of this contribution, but the inferred timing of cooling initiation from the detrital data alone is consistent with that from the in situ data, but lacks the same detail on later changes in cooling rate. Widespread Oligocene-Miocene (30-15 Ma) ZHe and AFT ages over a 2 km interval of elevation and the lack of younger ages in the northwest Santa Marta range have been used to infer this two-phase cooling, with deceleration taking place sometime in the last 15 My (Villagómez et al., 2011, Patiño et al., 2019).

4. Concluding statements

We have presented a method to infer thermal histories from detrital thermochronological data from a single catchment. We can model a hypothetical vertical profile, allowing for variations in control variables, such as annealing kinetics for AFT, and grain size for AHe, and then sample this according to a specified or inferred topographic sampling function (TSF). The detrital data can also be combined with in situ bedrock thermochronological data and this will yield more reliable inference of the TSF. In this contribution we use a least squares method to infer an optimal TSF for a given thermal history. At the expense of greater computational time, the TSF could also be sampled using a transdimensional McMC approach such as that applied to change point models (e.g. Gallagher et al. 2011, Fox et al. 2015). This would allow us to estimate credible intervals on the TSF for individual thermal histories.

In practice an inferred TSF will potentially reflect a combination of different factors, such as how erosion processes and production and transport of detrital material may vary with

484 elevation and also lithological controls on fertility and mineral fractionation/destruction
485 during transport. Depending on the scientific question of interest, the resolution of these
486 different contributing factors will require more detailed study of lithological compositions and
487 yield, and independent constraints on recent erosion rates (e.g. ^{10}Be, Fox et al . 2015)

488 A key assumption is that the thermal history is effectively the same across the
489 catchment and it is this thermal history that is represented in a catchment outlet detrital
490 sample. This could be relaxed to allow, for example, for a major fault in catchment by having
491 different thermal histories either side of the fault. This scenario then introduces more
492 complexity to the modelling process, as we need to infer the contributions from each side
493 present in a single detrital sample. Detrital sampling in upstream tributaries on both sides of
494 fault may provide additional information to help constrain the contributions in the outlet
495 sample. Overall, we suggest the approach as presented is best suited to small, confined
496 catchments with one major outlet, such as the Fundación catchment example we present here.
497 We have considered only single grain detrital data with unknown specific source regions
498 within the watershed (e.g. collected from a sand). Using aliquots of single grains separated
499 from pebbles or clasts (e.g. Fitzgerald et al. 2019) may be a useful extension of this approach
500 as such each aliquot will necessarily come from the same source region in the catchment.
501 Recent developments in analytical methods such LA-ICP-MS methods for fission track and
502 He dating provide additional data such as apatite U-Pb ages and REE spectra for the same
503 grains used for detrital thermochronology. Such data would also provide independent
504 information on potential source regions within a catchment, particularly if combined with
505 similar data from in situ samples. Finally, the approach we have presented could, in principle,
506 be applied to older sediments. However, in the absence of bedrock thermochronometry (and
507 other independent detrital source rock data), the TSF will clearly be less well constrained. To
508 estimate the TSF, we also need to specify the effective elevation range sampled by the

sediments. The structure of the inferred TSF will depend on that range and is validity difficult to assess in the absence of information on the proportions and fertility of different source rock lithologies. Also, we would also need to allow for the post-depositional thermal history. If the sediments have not been buried deep enough to sample the relevant partial annealing or retention zones, then this may have a relatively minor effect in terms of recovering the pre-depositional thermal history. However, increasing burial depth will progressively overprint the provenance related signal, reducing the resolution of the pre-depositional thermal history to perhaps just the time the grains in the sediment cooled below the effective closure temperature, or entered the partial annealing or retention zones.

Acknowledgements

We would like to thank Nathan Niemi and Matthew Fox for useful reviews that helped us clarify certain aspects of this paper. Also we thank Maxime Bernard, Juan Sebastián Echeverri, Ana María Patiño, Philippe Steer, and Peter van der Beek for comments and discussion over the last year or so. This work was facilitated through a FAPESP-CNRS binational project (FAPESP Sprint 2017/ 50276-3). M.P thanks FAPESP JP Project 2013/03265-5 for funding the data acquisition.

References

Avdeev B., Niemi, N., Clark, M.K., 2011. Doing more with less: Bayesian estimation of erosion models with detrital thermochronometric data Earth. Planet. Sci. Letts., 305, 385-395.

Brandon, M.T., 1996. Probability plots for fission-track grain-age samples, Rad. Meas., 26, 663-676.

Braun, J., Gemignani, L., van der Beek, P., 2018. Extracting information on the spatial variability in erosion rate stored in detrital cooling age distributions in river sands. Earth Surf. Dyn. 6, 257–270. https://doi.org/10.5194/esurf-6-257-2018.

Braun, J., van der Beek, P., Valla, P., Robert, X., Herman, F. Glotzbach,C., Pedersen, V., Perry,C., Simon-Labric,T. Prigent C. 2012. Quantifying rates of landscape evolution and tectonic processes by thermochronology and numerical modeling of crustal heat transport using PECUBE. Tectonophysics, 524-525, 1-28

Brewer, I.D., Burbank, D.W., Hodges, K.V., 2003. Modelling detrital cooling-age populations: insights from two Himalayan catchments, Basin Res. 15, 305-320.

Brown, R.W., Beucher, R., Roper, S., Persano, C., Stuart, F., Fitzgerald, P., 2013. Natural age dispersion arising from the analysis of broken crystals, part I. Theoretical basis and implications for the apatite (U-Th)/He thermochronometer. Geochimica et Cosmochimica Acta, 122. 478-497.

Carter A, Bristow C.S., 2000. Detrital zircon geochronology: Enhancing the quality of sedimentary source information through improved methodology and combined U-Pb and fission-track techniques. Basin Res., 12, 47-57

Copeland, P. and Harrison, T.M., 1990. Episodic rapid uplift in the Himalaya revealed by $^{40}Ar/^{39}Ar$ analysis of detrital K-feldspar and muscovite, Bengal Fan. Geology 18**,** 354-357.

Dodson, M. H, 1973. Closure temperature in cooling geochronological and petrological systems, Contrib. Mineral. Petrol., 40, 259–274.

Ehlers, T. A., Szameitat, A., Enkelmann, E., Yanites, B. J., Woodsworth, G. J., 2015., Identifying spatial variations in glacial catchment erosion with detrital thermochronology, J. Geophys. Res. Earth Surf., 120, 1023–1039, doi:10.1002/ 2014JF003432.

Ehlers, T.A., Farley, K.A., Rusmore, M.E ., and Woodsworth, G.J., 2006, Apatite (U- Th)/He signal of large-magnitude accelerated glacial erosion, southwest British Columbia. Geology, v. 34, p. 765-768.

Enklemann, E. and Ehlers, T.A., 2015. Evaluation of detrital thermochronology for quantification of glacial catchment denudation and sediment mixing. Chem. Geol., 411 299–309

Farley K.A., 2000. Helium diffusion from apatite: general behavior as illustrated by Duragno fluorapatite. J Geophys Res 105, 2903-2914

Fitzgerald, P. G., Sorkhabi, R. B., Redfield T. F., Stump E., 1995. Uplift and denudation of the central Alaska Range: A case study in the use of apatite fission-track thermo-chronology to determine absolute uplift parameters. J. Geophy. Res., 100, 20175–20191.

Fitzgerald, P.G., Malusà, M.G. Muñoz, J.A., 2019. Detrital thermochronology using conglomerates and cobbles IN : Malusà, , M.G. and Fitzgerald, P.G. (Editors), Fission-Track Thermochronology and its Application to Geology, Springer International Publ. AG, 295-314.

572 Flowers, R.M., Ketcham, R.A., Shuster, D.L., Farley, K.A. 2009. Apatite (U-Th)/He
573 thermochronometry using a radiation damage accumulation and annealing model.
574 Geochimica et Cosmochimica Acta, 73, 2347-2365.

575 Fox, M., Herman, F., Willett, S.D., May, D.A., 2014. A linear inversion method to infer
576 exhumation rates in space and time from thermchronological data, Earth Surf. Dynam., 2,
577 47-65.

578 Fox, M., Leith, K., Bodin, T., Balco, G. and Shuster, D.L., 2015. Rate of fluvial incision in
579 the Cen tral Alps constrained through joint inversion of detrital ^{10}Be and
580 thermochronometric data. Earth Planet. Sci. Letts., 411., 27-36.

581 Galbraith, R.F., 2005., Statistics for Fission Track Analysis; Chapman and Hall/CRC, 240 p.

582 Gallagher, K. 1995. Evolving thermal histories from fission track data, Earth Planet. Sci.
583 Letts., 136, 421-435.

584 Gallagher, K., 2012. Transdimensional inverse thermal history modelling for quantitative
585 thermochronology, J. Geophys Res. 117, B02408, doi:10.1029/2011JB00882.

586 Gallagher, K., Bodin, T. Sambridge, M, Weiss, D, Kylander, M, Large, D., 2011. Inference of
587 abrupt changes in noisy geochemical records using Bayesian transdimensional
588 changepoint models, Earth Planet. Sci. Letts., 311, 182-194.

589 Gallagher, K., Stephenson, J., Brown R., Holmes, C. Fitzgerald, P. 2005. Low temperature
590 thermochronology and modelling strategies for multiple samples 1 : vertical profiles,
591 Earth Planet Sci. Letts., 237, 193-208.

592 Garver J.I., Brandon M.T., 1994. Fission-track ages of detrital zircon from Cretaceous strata,
593 southern British Columbia: Implications for the Baja BC hypothesis. Tectonics 13, 401-
594 420

595 Gautheron, C., Tassan-Got, L., Barbarand, J., Pagel, M. 2009. Effect of alpha-damage
596 annealing on apatite (U-Th)/He thermochronology. Chemical Geology, 266, 157-170.

597 Gemignani, L., van der Beek, P.A., Braun, J. Najman,Y. ,Bernet, M. , Garzantie, E. and
598 Wijbrans, J.R., 2018. Downstream evolution of the thermochronologic age signal in the
599 Brahmaputra catchment (eastern Himalaya): Implications for the detrital record of
600 erosion. Earth. Planet. Sci. Letts., 499, 48-61.

601 Gómez, J., Montes, N.E., Nivia, Á. & Diederix, H., compilers. 2015. Geological Map of
602 Colombia 2015. Scale 1:1 000 000. Servicio Geológico Colombiano, 2 sheets. Bogotá.

603 Green P.F., 1988. The relationship between track shortening and fission track age reduction in
604 apatite: combined influences of inherent instability, annealing anisotropy, length bias and
605 systems calibration. Earth Planet Sci Lett 89, 335-352

606 Green P.F., Duddy I.R., Laslett G.M., Hegarty K.A., Gleadow A.J.W., Lovering J.F. 1989.
607 Thermal annealing of fission tracks in apatite 4. Quantitative modeling techniques and
608 extension to geological timescales. Chem Geol 79, 155-182

609 Huntington, K. W., Hodges, K.V. 2006. A comparative study of detrital mineral and bedrock
610 age-elevation methods for estimating erosion rates, J. Geophys. Res., 111, F03011,
611 doi:10.1029/2005JF000454.

612 Hurford, A. J., and Green, P. F., (1983), The zeta age calibration of fission-track dating:
613 Isotope Geoscience, v. 1, no. 4, p. 285-317.

614 Ketcham, R.A., Carter, A., Donelick, R.A., Barbarand, J., Hurford, A.J., .2007. Improved
615 modeling of fission-track annealing in apatite. American Mineralogist 92, 799–810.

Ketcham, R.A., Donelick, R.A., Carlson,W.D., (1999). Variability of apatite fission-track annealing kinetics. III. Extrapolation to geological timescales. American Mineralogist 84, 1235–1255.

Kim, D., Sra, S., Dhillon, I.S., 2013., A non-monotonic method for large-scale non-negative least squares. Optimization Meth. & Software, 28, 1012-1039.

Malusà, M.G. and Garzanti, E. 2019. The Sedimentology of Detrital Thermochronology, IN : Fission-Track Thermochronology and its Application to Geology, Malusà, M.G. and Fitzgerald; P.. (Editors) 123-143

Malusà, M.G. and Fitzgerald, P.G. 2019. Application of Thermchronology to Geologic Problems : Bedrock and Detrital Approaches, IN : Malusà, , M.G. and Fitzgerald, P.G. (Editors), Fission-Track Thermochronology and its Application to Geology, Springer International Publ. AG, 191-200.

Parra, M., Echeverri, S., Patiño, A.M., Ramírez-Arias, J.C., Mora, A., Sobel, E.R., Almendral, A., Pardo, A., in press, Cenozoic Evolution of the Sierra Nevada de Santa Marta, In: Gómez Tapias, J., Almanza, M.F., Ochoa, A. (eds), The Geology of Colombia Book, Servicio Geológico Colombiano.

Patiño, A. M., Parra, M., Ramírez, J. C., Sobel, E. R., Glodny, J., Almendral, A., and Echeverri, S., (2019), Thermochronological constraints on Cenozoic exhumation along the southern Caribbean: The Santa Marta range, northern Colombia, in Horton, B. K., and Folguera, A., eds., Andean Tectonics, Elsevier, p. 103-132. Read, A.L. 1999. Linear interpolation of histograms, Nucl. Instr. and Methods in Physics Res. A 425, 357-360.

Reiners, P.W., Ehlers, T.A., 2005. Low-Temperature thermochronology : Techniques, Interpretations, and Applications. Reviews in Mineralogy and Geochemistry, v. 58, 1. Min. Soc. Am. Geochem Soc.

Ross., GH.M., Bowring, S.A., 1990. Detrital Zircon Geochronology of the Windermere Supergroup and the Tectonic Assembly of the Southern Canadian Cordillera , J. Geology, 98, 879-893.

Ruhl, K.W., Hodges, K.V., 2005. The use of detrital mineral cooling ages to evaluate steady state assumptions in active orogens: An example from the central Nepalese Himalaya. Tectonics 24, 1-14.

Schoene, B. (2014) U–Th–Pb Geochronology, Treatise on Geochemistry , Volume 4 : the Crust, Ch. 4.10, 341-378.

Stock, G.M., Ehlers, T.A., Farley, K.A., 2006. Where does sediment come from? Quantifying catchment erosion with detrital apatite (U–Th)/He thermochronometry. Geology 34, 725–728.

Tranel, L.M. Spotila, J.A., Kowalewski, M.J., Waller, C.M. 2011. Spatial variation of erosion in a small glaciated basin in the Teton Range, Wyoming, based on detrital apatite (U-Th)/He thermochronology. Basin Research, 23, 571-590.

Valla, P.G., Herman., F., van der Beek, P.A., Braun, J., 2010. Inversion of thermochronological age-elevation profile to extract independent estimates of denudation and relief history I: Theory and conceptual model, Earth Planet. Sci. Letts., 295, 511-522

Villagomez, D., Spikings, R;, Mora, A., Guzman, G., Ojeda, G.,n, Cortés, E;, van der Lelij, R. 2011. Vertical tectonics at a continental crust- oceanic plateau plate boundary zone: Fission track thermochronology of the Sierra Nevada de Santa Marta, Colombia, Tectonics, 30, TC4004, doi:10.1029/2010TC002835

Wagner G.A., Reimer G.M., 1972. Fission track tectonics: The tectonic interpretation of fission track apatite ages, Earth Planet. Sci. Letts. 14(2), 263-268.

Wagner G.A., Reimer G.M., Jager E., 1977. Cooling ages derived by apatite fission track, mica Rb-Sr, and K-Ar dating: the uplift and cooling history of the central Alps. Mem. Inst. Geol. Mineral. Univ. Padova 30:1–27

Whipp, D. M., Jr., Ehlers, T.A., Braun, J., Spath, C. D. 2009. Effects of exhumation kinematics and topographic evolution on detrital thermochronometer data, J. Geophys. Res., 114, F04021, doi:10.1029/2008JF001195.

Willett, C.D., Fox, M., Shuster, D.L., 2017. A helium-based model for the effects of radiation damage annealing on helium diffusion kinetics in apatite. Earth. Planet. Sci. Letts., 477, 195-204.

Figure Captions

Figure 1.

The conceptual model to predict detrital distributions for thermochronological data.

(a) Yellow stars represent a typical in situ or bedrock vertical profile, that may not cover the whole elevation range in a catchment. The green star represents a modern sediment detrital sample from the outlet of the catchment. To model the detrital sample, we use a set of hypothetical of dummy samples spanning the total elevation range of the catchment.

Given a specified thermal history (b), and the hypothetical samples, we can predict an age elevation profile (c) for AFT and AHe (and similarly for track length distributions, not shown), using a range of control variables (CV). These are kinetic parameters for AFT and grain size for AHe. In practice the control variables are defined from the values and groups defined for a real detrital sample. This allows us to produce a set of AHe and AFT ages for the dummy samples at each elevation. Note that these predictions do not contain any statistical dispersion.

(d) By resampling the predicted ages for each control group variable at each elevation 50-100 times and adding expected statistical variations, we can produce a distribution of ages for each control group variable. These are then summed, weighted by the specified proportion of each CV group (the thick line in (d)).

(e) We produce CV weighted distributions for each elevation

(f) These are summed over the elevation range and weighted by the topographic sampling function (TSF) to give a prediction of the detrital distribution for AHe and AFT at the outlet of the catchment.

Figure 2.

(a) Location of in situ (blue circles) and detrital (yellow circle) samples, with the AFT centrals ages, recalculated from the data of Villagomez et al. (2011), in the Fundación catchment (black outline) and a geological map (modified from Gómez et al. 2015) for the Santa Marta de Sierra Nevada, northern Colombia. SMB = Santa Marta Boundary fault.

(b) Present day distribution of elevation (SRTM 90m), or hypsometry, in the Fundación catchment. The black line is a running mean, and the red line is the cumulative distribution of elevation.

Figure 3.

(a) Inferred thermal history from just in situ bed rock samples from the Fundación catchment. The blue and red lines indicate the thermal histories for the uppermost and lowermost elevation bedrock samples, with the 95% credible range on each. The grey lines are for other in situ samples in the vertical profile, while the yellow lines are thermal histories for dummy samples. The red box is the prior distribution for time-temperature points, and the black box is an initial constraint to force the thermal history to start at a temperature the total annealing/degassing temperatures for fission tracks and He in apatite.

(b) Observations and predictions using the thermal history in (a). Blue circles = observed AFT ages, red diamonds = observed AFT Mean track length (MTL). The predictions are shown by the dashed lines. The predicted AFT ages also include those for the dummy samples and the horizontal lines show the 95% credible range on the predicted age at each elevation for all accepted thermal histories.

(c) Predicted detrital AFT age distribution using the thermal history in (a), assuming the topographic sampling function (TSF) is the present day hypsometry (see figure 2). The histogram and light blue line represent the observed detrital AFT ages. The red line is the predicted distribution for the thermal history in (a), and the black line is the average of the predicted detrital distributions for all accepted thermal histories.

Figure 4

(a) Inferred thermal history from just the detrital sample at the outlet of the Fundación catchment. See the caption for figure 3 for more details.

(b) Observations and predictions using the thermal history in (a).

(c) Predicted detrital AFT age distribution using the thermal history in (a), assuming the topographic sampling function (TSF) is the present day hypsometry.

Figure 5

(a) Inferred thermal history from both the in situ samples and the detrital sample at the outlet of the Fundación catchment. See the caption for figure 3 for more details.

(b) Observations and predictions using the thermal history in (a).

(c) Predicted detrital AFT age distribution using the thermal history in (a), assuming the topographic sampling function (TSF) is the present day hypsometry.

Figure 6

(a) Inferred thermal history from both the in situ samples and the detrital sample at the outlet of the Fundación catchment, allowing for the TSF to be different to the present day hypsometry. See the caption for figure 3 for more details.

(b) Observations and predictions using the thermal history in (a) and the inferred TSF shown in (c).

(c) Predicted detrital AFT age distribution using the thermal history in (a), together with the inferred TSF, estimated with a non-negative least squares method, using the present day hypsometry as a starting model. See main text for details.

Figure 1

Click here to download Figure: Figure 1.pdf

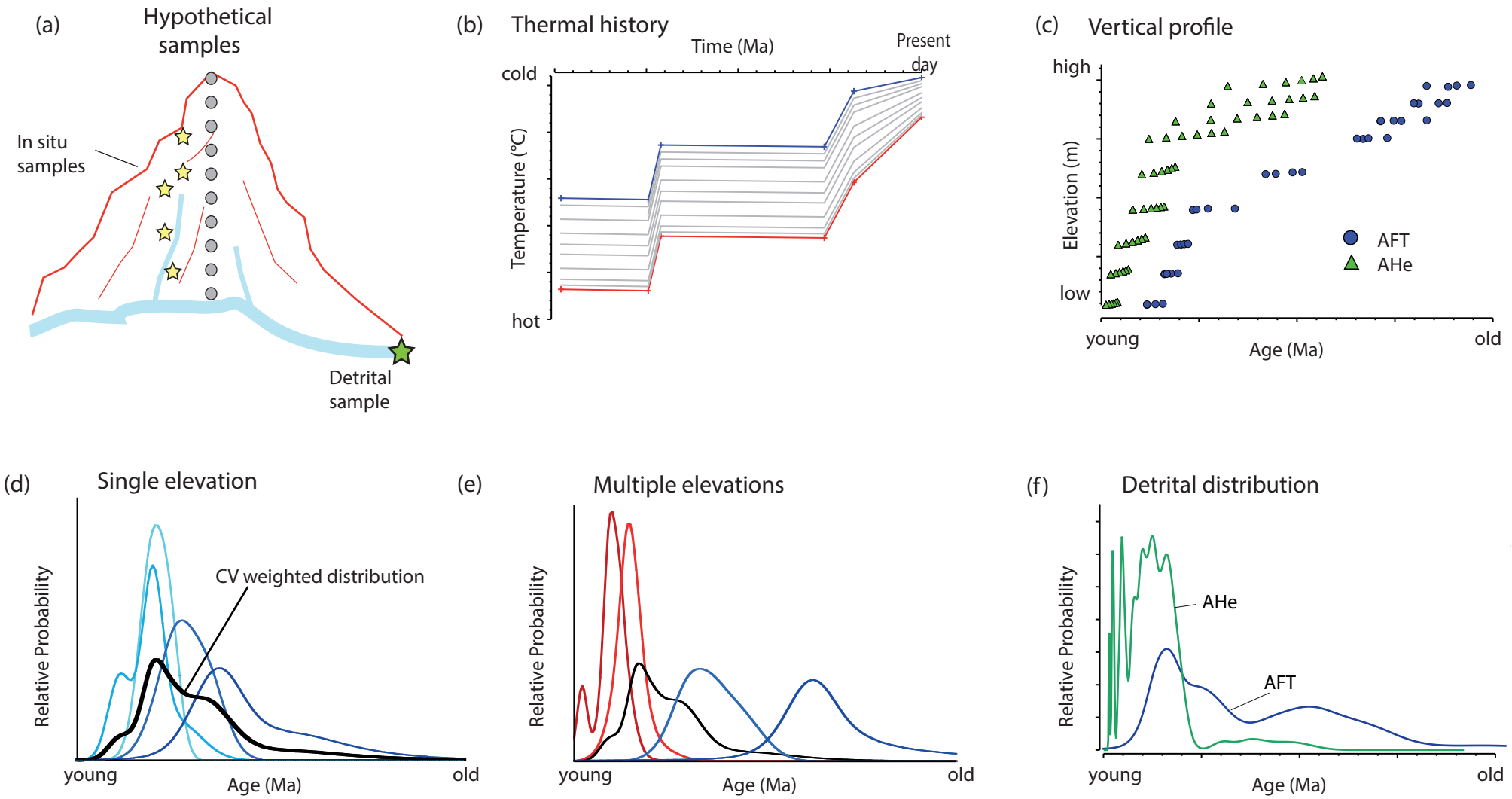

Figure 1

Figure 2

Click here to download high resolution image

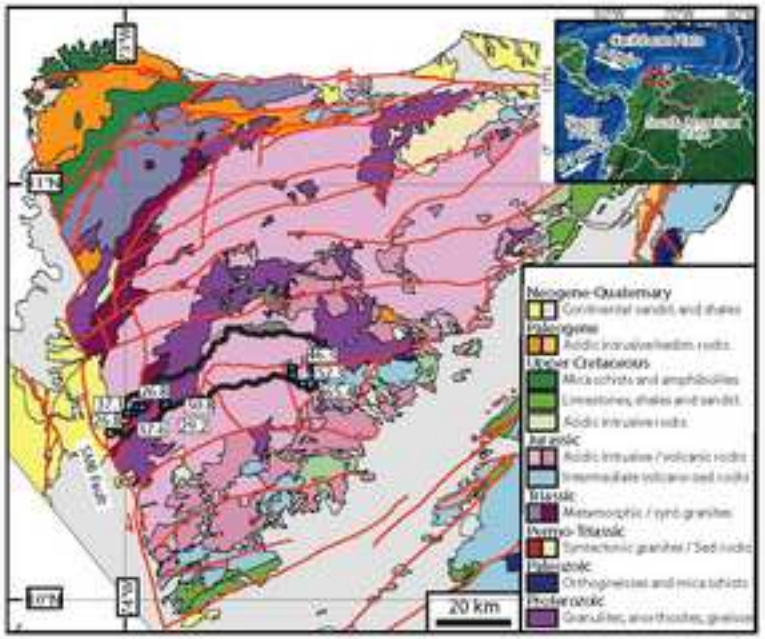

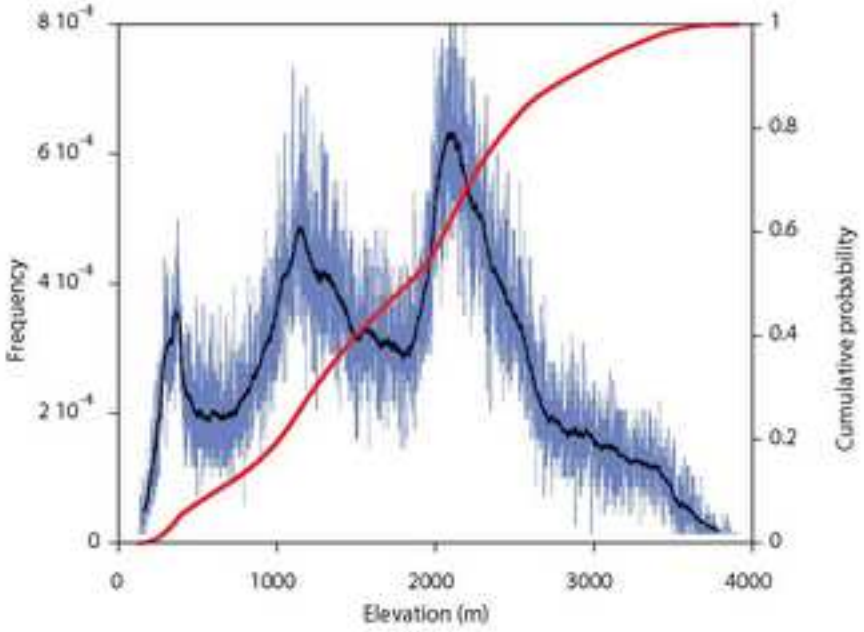

Figure 2

Figure 3

Click here to download Figure: Figure 3.pdf

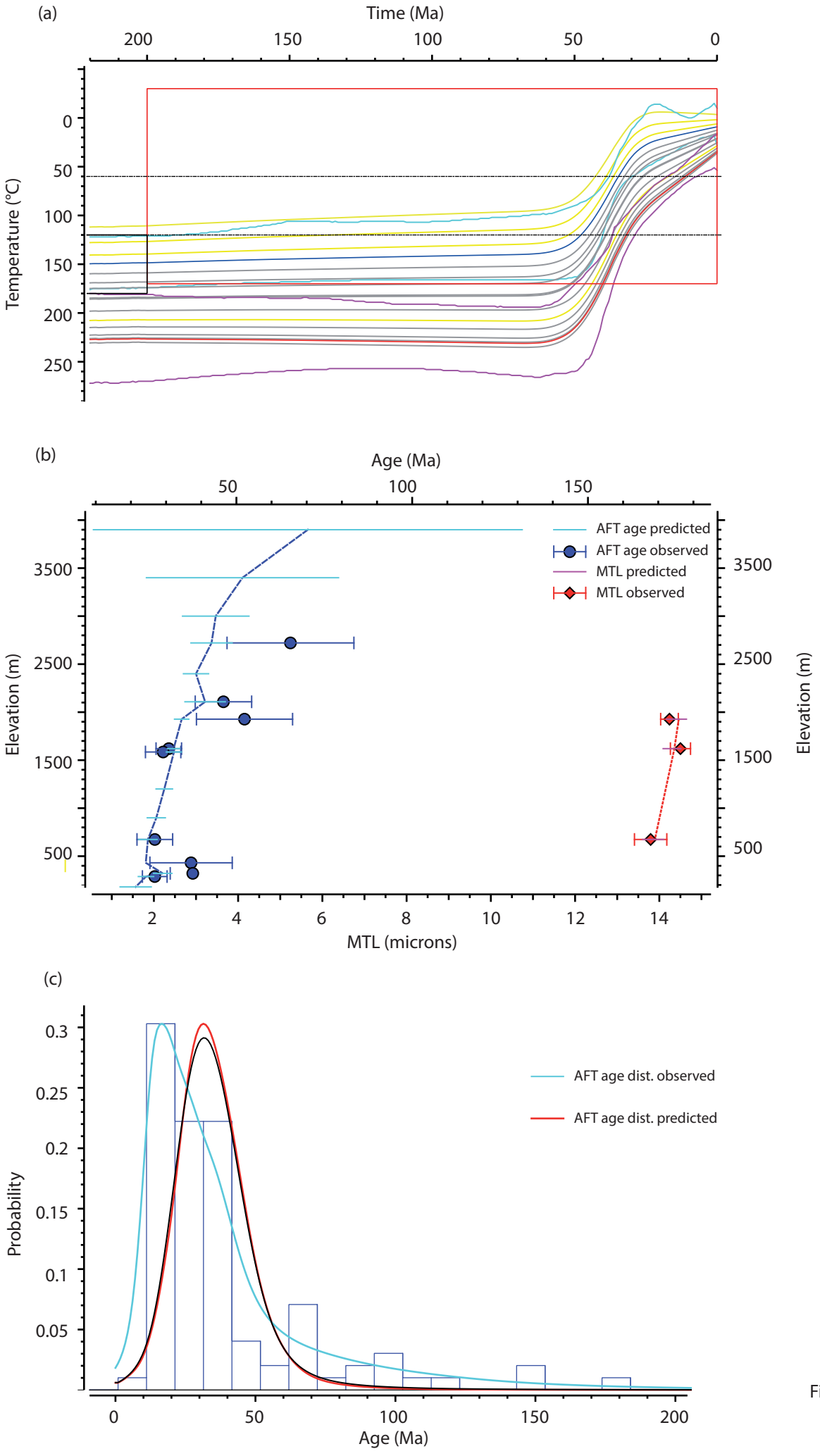

Figure 3

Figure 4

Click here to download Figure: Figure 4.pdf

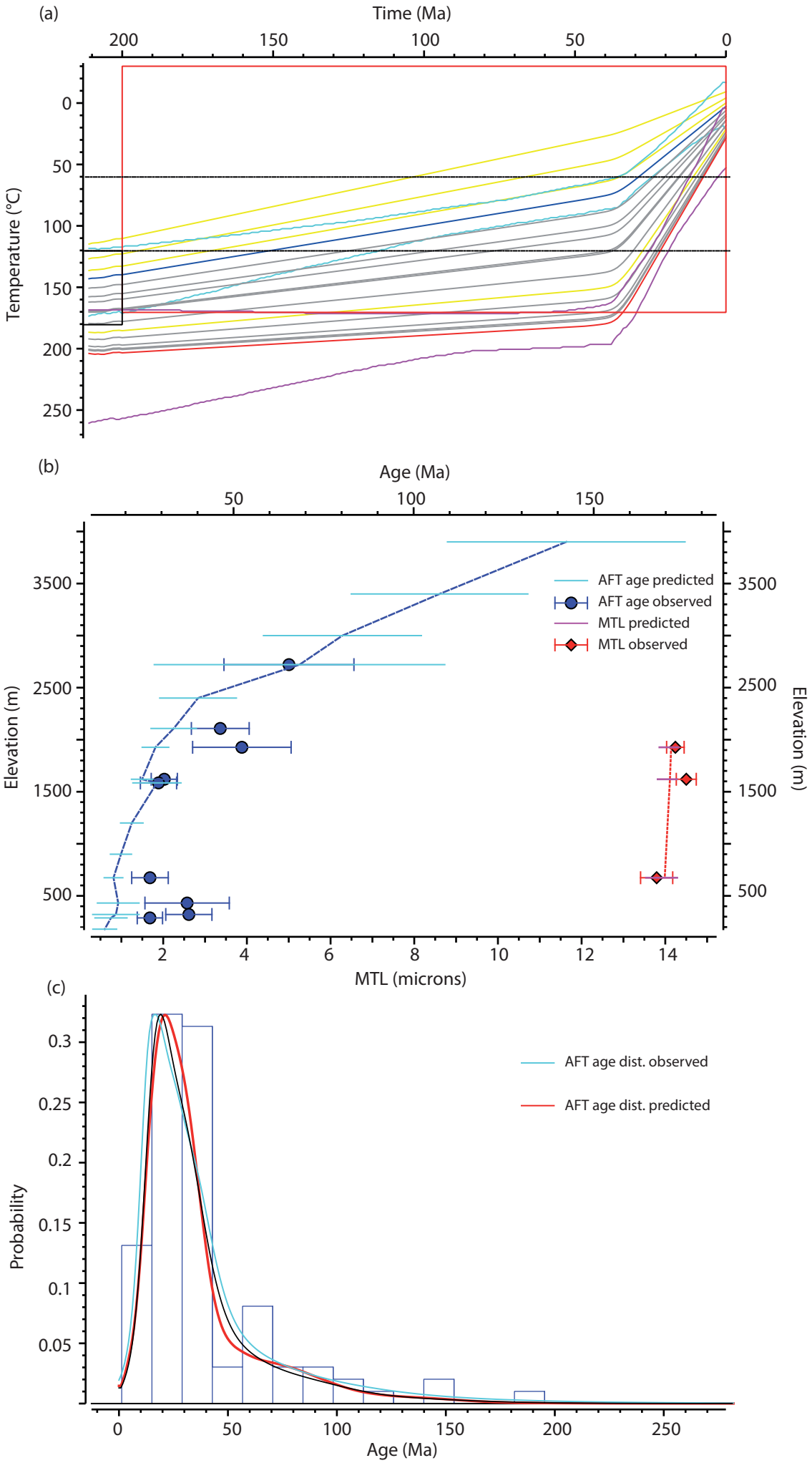

Figure 4

Figure 5

Click here to download Figure: Figure 5.pdf

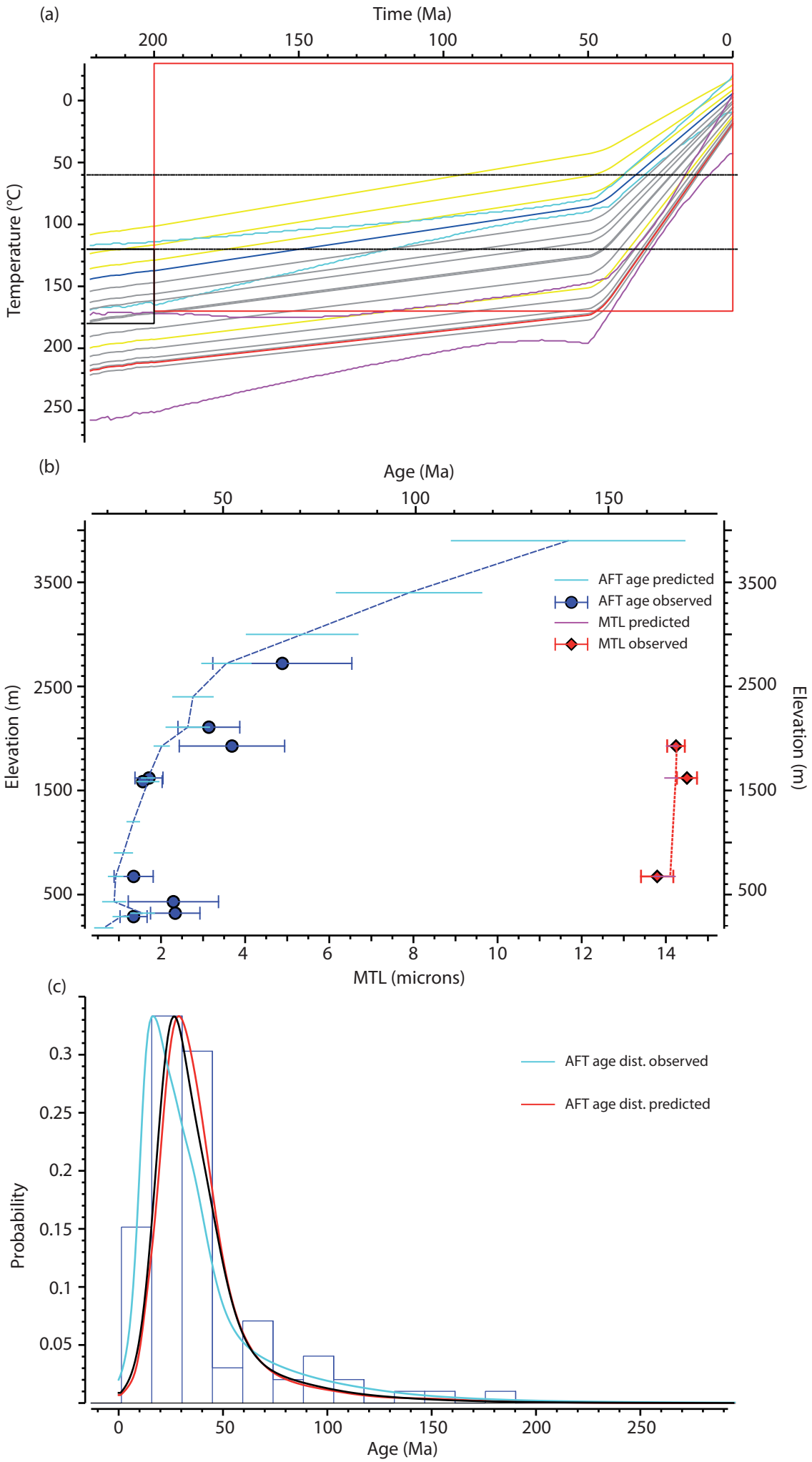

Figure 5

Figure 6

Click here to download Figure: Figure 6.pdf

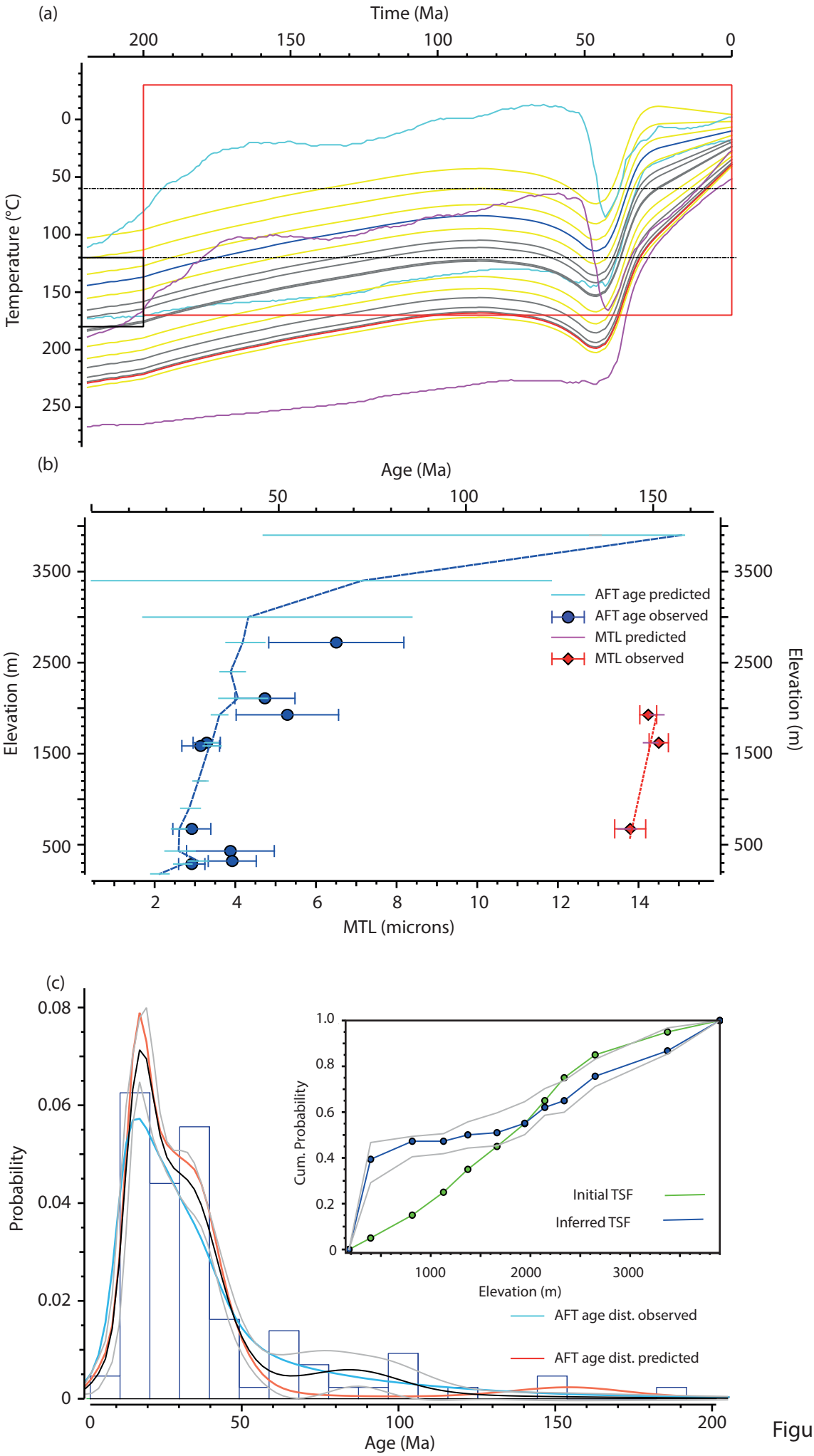

Figure 6

Figure 2 (high-resolution)

Click here to download Figure (high-resolution): Figure 2_(high res).pdf

Supplementary material for online publication only

Click here to download Supplementary material for online publication only: Gallagher_Parra_Supplementary Material.docx